

Optical spectrum of ferrovalley materials: A case study of Janus H-VSSe

Chao-Bo Luo(罗朝波), Wen-Chao Liu(刘文超), and Xiang-Yang Peng(彭向阳)
Citation: Chin. Phys. B, 2024, 33 (**1**): 016303. DOI: 10.1088/1674-1056/acf660
Journal homepage: http://cpb.iphy.ac.cn; http://iopscience.iop.org/cpb

What follows is a list of articles you may be interested in

Determining Hubbard *U* of VO_2 by the quasi-harmonic approximation

Longjuan Kong(孔龙娟), Yuhang Lu(陆雨航), Xinying Zhuang(庄新莹), Zhiyong Zhou(周志勇), and Zhenpeng Hu(胡振芃)
Chin. Phys. B, 2024, 33 (**1**): 016302. DOI: 10.1088/1674-1056/acfd18

Straight and twisted Weyl nodal line phonons in Ho_2CF_2 material

Xin-Yue Kang(康鑫越), Jin-Yang Li(李金洋), and Si Li(李思)
Chin. Phys. B, 2023, 32 (**11**): 116301. DOI: 10.1088/1674-1056/aceaea

Evaluating thermal expansion in fluorides and oxides: Machine learning predictions with connectivity descriptors

Yilin Zhang(张轶霖), Huimin Mu(穆慧敏), Yuxin Cai(蔡雨欣), Xiaoyu Wang(王啸宇), Kun Zhou(周琨), Fuyu Tian(田伏钰), Yuhao Fu(付钰豪), and Lijun Zhang(张立军)
Chin. Phys. B, 2023, 32 (**5**): 056302. DOI: 10.1088/1674-1056/accdca

Evaluation of performance of machine learning methods in mining structure—property data of halide perovskite materials

Ruoting Zhao(赵若廷), Bangyu Xing(邢邦昱), Huimin Mu(穆慧敏), Yuhao Fu(付钰豪), and Lijun Zhang(张立军)
Chin. Phys. B, 2022, 31 (**5**): 056302. DOI: 10.1088/1674-1056/ac5d2d

Inverted V-shaped evolution of superconducting temperature in SrBC under pressure

Ru-Yi Zhao(赵如意), Xun-Wang Yan(闫循旺), and Miao Gao(高淼)
Chin. Phys. B, 2021, 30 (**7**): 076301. DOI: 10.1088/1674-1056/abfbcc

---

SPECIAL TOPIC — Valleytronics

Optical spectrum of ferrovalley materials: A case study of Janus H-VSSe

Chao-Bo Luo(罗朝波), Wen-Chao Liu(刘文超), and Xiang-Yang Peng(彭向阳)†

Hunan Key Laboratory for Micro-Nano Energy Materials and Devices, School of Physics and Optoelectronics, Xiangtan University, Xiangtan 411105, *China*

(Received 31 May 2023; revised manuscript received 13 August 2023; accepted manuscript online 4 September 2023)

As opposed to the prototypical MoS_2 with centroasymmetry, Janus ferrovalley materials such as H-VSSe are less symmetric with the mirror symmetry and time reversal symmetry broken, and hence possess spontaneous valley polarization and strong ferroelasticity. The optical transition is an important means to excite the valley carriers. We investigate the optical spectrum of H-VSSe by using the many-body perturbation-based GW approach and solving the Bethe–Salpeter equation (BSE) to include the electron–hole interactions. It is found that after the GW correction, the band gaps of the quasiparticle bands are much larger than those obtained by the normal density functional theory. The system is ferromagnetic and the valley gaps become non-degenerate due to spin–orbit coupling (SOC). The position of the lowest BSE peak is much lower than the quasiparticle band gap, indicating that the excitonic effect is large. The peak is split into two peaks by the SOC. The binding energy difference between these two BSE peaks is about the same as the difference between the inequivalent valley gaps. Our results show that in Janus H-VSSe the two lowest exciton peaks are from the two inequivalent valleys with different gaps, in contrast to the A and B exciton peaks of MoS_2 which are from the same valley.

Keywords: valleytronics, first-principles calculations, GW approach and Bethe–Salpeter equation (GW-BSE), excitonic effects

PACS: 63.20.dk, 71.20.–b, 71.35.Cc **DOI:** 10.1088/1674-1056/acf660

1. Introduction

Valleytronics materials have inequivalent gapped valleys in the Brillouin zone, formed by pairs of extrema in the conduction and valence band edges at the same k-points.[1–3] The H phase monolayer transition metal dichalcogenides, e.g., MoS_2, WSe_2, are found to be excellent valleytronic materials with direct band gaps located at the valleys in the energy range of visible light.[4–6] Since the space inversion symmetry is broken, valleytronic materials have opposite Berry curvatures at the inequivalent valleys, leading to various quantum phenomena, such as valley-dependent light selection rules and valley Hall effect.[1] The electrons in the K and $-K$ valleys can only absorb light with opposite circular polarization. This valley dependent optical selection rule provides an approach to the realization of the valley polarization and can be applied in information encoding. Therefore, it is important to study the optical properties of valleytronic materials.

In non-magnetic valleytronic materials, e.g., MoS_2, the energy gaps of the inequivalent valleys have the same magnitude. The inequivalent valley gaps become different if the time reversal symmetry is broken by, e.g., adding a magnetic field,[7,8] doping magnetic atoms,[9,10] or forming a heterojunction with a magnetic substrate to realize valley polarization.[11–14] However, the resulting difference in the gaps is quite small by these means. In ferromagnetic valleytronic materials, e.g., VSe_2,[15,16] the difference of the inequivalent gaps is much larger, leading to an intrinsic difference of charge occupancy in the valleys and hence resulting in the spontaneous valley polarization. The latter are called ferrovalley materials, which can be applied in non-volatile valleytronic devices. Due to the unequal gaps at the inequivalent valleys, the optical properties of ferrovalley materials should be distinct from the normal valleytronic materials, which are still to be addressed.

Recently, more and more ferrovalley materials have been discovered, such as H-VSe_2,[15,16] H-$LaBr_2$,[17] H-GdI_2,[18] H-$FeCl_2$,[19,20] Nb_3I_8,[21] MN_2H_2[22] and VSi_2N_4[23,24] and their Janus structures,[9,25–31] in which not only the spatial inversion symmetry but also the time reversal symmetry is broken. Ferrovalley materials are promising materials for spintronic and valleytronic devices, but the optical properties of ferrovalley materials in terms of exciton effects have yet to be studied. In Janus ferrovalley materials, the symmetry is further lowered by breaking the mirror symmetry. Theoretical calculations show that Janus H-VSSe is a multiferroic material with ferroelasticity, ferromagnetism and ferrovalley. It has been shown to have dynamically and thermodynamically stable, and its valleytronic properties are well tunable.[25,28,32] In this work, we will take H-VSSe as an example of the ferrovalley materials to study its optical properties. The influences of ferromagnetism, valley polarization and spin–orbital coupling on the electronic structure and exciton spectrum will be inves-

†Corresponding author. E-mail: xiangyang_peng@xtu.edu.cn

© 2024 Chinese Physical Society and IOP Publishing Ltd

tigated.

There have been experimental and theoretical researches on the optical properties of valleytronic materials. In computational studies, in order to accurately calculate the band gap, it is necessary to go beyond the normal density functional theory (DFT), since it usually considerably underestimates the band gap. After the optical transition, the electron jumping to the conduction band will interact with the hole it leaves in the valence band, and the electron–hole binding energy will significantly affect the optical spectrum if the screening is not effective. In two dimensional materials, the screening is usually weak due to its finite size along the direction normal to the plane. In previous studies, the optical properties of valleytronic materials, e.g., MoS_2, WS_2 and WSe_2,[4–6] have been calculated. In the case of monolayer MoS_2, the calculated DFT bandgap is about 1.60 eV,[5] whereas the calculated GW bandgap gives a much larger value of 2.84 eV,[4] indicating the many-body correction is large. To address the band gap problem in DFT, the GW method based many body perturbation is used in this study. To account for the effects of electron–hole interaction on the optical spectrum, Bethe–Salpeter equations (BSE) are solved on top of the GW calculations. The first peak in the BSE dielectric function (absorption spectrum) is located at 1.88 eV,[4] in good agreement with the experimental photoluminescence spectroscopy.[33] The position of the first peak by BSE (1.88 eV) is much smaller than the band gap (2.84 eV), which suggests that the electron–hole interaction is strong and hence cannot be ignored in the study of the optical properties of valleytronic materials. Therefore, in the following study of monolayer H-VSSe, we use the GW plus BSE approach to describe the many body effect and use the electron–hole interaction to give more accurate and reliable predictions of the optical properties.

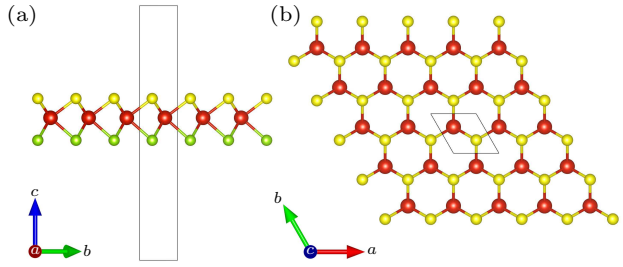


Fig. 1. The side and top views of Janus H-VSSe. The red, green and yellow spheres represent the V, Se, and S atoms, respectively.

2. Methods

The first-principles calculations are carried out using the Vienna *ab initio* simulation package (VASP),[34,35] with generalized gradient approximation in the form of Perdew–Burke–Ernzerhof (PBE) functional.[36] The projector augmented wave (PAW) potentials are employed to describe the core–electron interaction. A total of 23 electrons in V (p, d and s orbitals), S (s and p orbitals) and Se (s and p orbitals) atoms are taken as valence electrons in the pseudopotentials. The electron wave functions are expanded by plane waves with an energy cutoff of 300 eV. Our tests show that the cut-off energies of 300 eV and 400 eV yield almost the same results. In order to minimize the influence of the periodic images, a vacuum layer larger than 15 Å is added between the slabs. The effect of spin–orbit coupling is considered in the calculation. In the Brillouin zone, a series of Γ-centered k-grids have been evaluated up to $15 \times 15 \times 1$. Hybrid functional calculations are further carried out using the Heyd–Scuseria–Ernzerhof exchange–correlation functional (HSE06),[37] based on which the partially self-consistent GW[38] calculations are performed including 192 orbitals (169 empty orbitals). In order to obtain quasiparticle energy bands, the Wannier90 package is used for interpolation fitting,[39] and the d orbitals of V atoms and the p orbitals of S and Se atoms are selected for initial projection, with a total of 22 electron orbitals. The Berry curvature of the valence bands of H-VSSe is obtained by the Wannier90 package. Finally, the Bethe–Salpeter equations are solved on top of GW, with the eight highest valence bands and eight lowest conduction bands taken as the basis of the excitonic state, and the optical absorption spectrum is obtained.

3. Results and discussion

3.1. Quasiparticle band structures of Janus H-VSSe

In our calculations, the lattice constant of H-VSSe is optimized to be 3.26 Å. As shown in Fig. 2, we calculate the band structures of Janus H-VSSe by using PBE, hybrid functional HSE06, and GW_0 methods, taking spin polarization into consideration. Among them, PBE bands and their Wannier interpolated bands almost coincide with each other, indicating that the selected projected orbitals are suitable. Although overall the H-VSSe has an indirect band gap, the bands of the same spin have two identical direct band gaps located at the K and $-K$ points, which are 0.7769 eV, 1.0299 eV and 1.4315 eV by PBE, HSE06 and GW_0 methods, respectively. The latter two gaps are significantly larger than the PBE gap, indicating that the ordinary DFT calculation considerably underestimates the band gap of H-VSSe. The GW_0 band gap is about twice as much as the PBE gap and 40% larger than that by HSE06, and therefore the quasiparticle effect in the two dimensional H-VSSe is strong. Regardless of the calculation methods, all the energy bands have valleys near the Fermi level at the K and $-K$ points. The band edges of the valleys are of the same spin polarization, showing that H-VSSe is a magnetic valleytronic material. The calculated magnetic moment per primitive cell is μ_B.

Since transition metal elements have strong spin–orbit coupling (SOC), we further take it into consideration in the

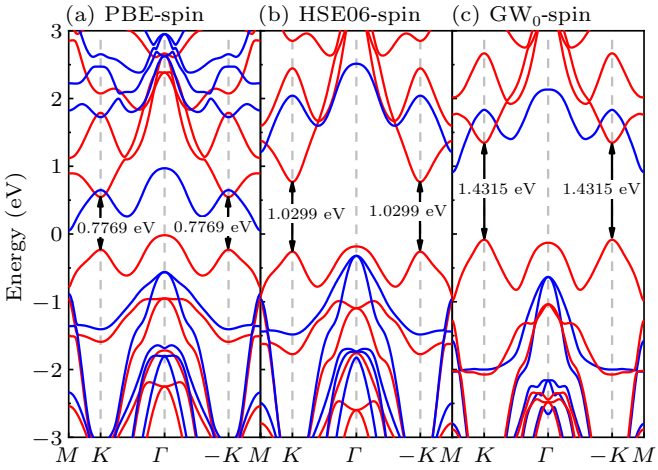


Fig. 2. The band structure of H-VSSe with ferromagnetism but without SOC. Panels (a)–(c) are calculated by PBE, HSE06 and GW$_0$, respectively.

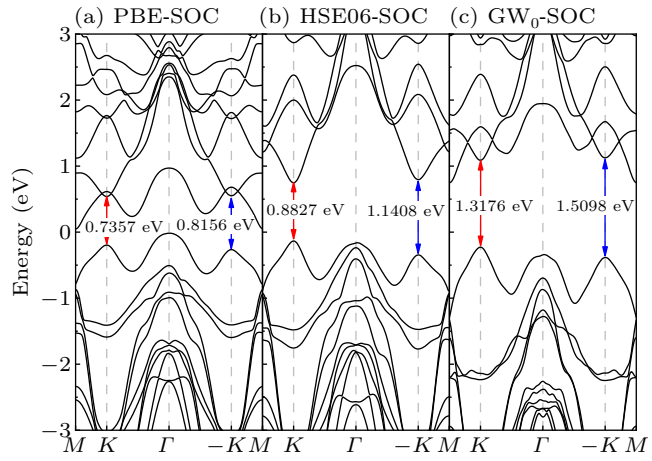


Fig. 3. The band structure of H-VSSe with ferromagnetism and SOC. Panels (a)–(c) are calculated by PBE, HSE06 and GW$_0$, respectively.

calculation and obtain band structures, as shown in Fig. 3. Similar to the bands without SOC, the SOC bands are also gapped at the K and $-K$ points. Without SOC, the gaps at the K and $-K$ valleys are degenerate (Fig. 2). After the introduction of SOC, the valley gap degeneracy is lifted as shown in Fig. 3. The valley gap at K is 0.736 eV (PBE), 0.883 eV (HSE06), and 1.318 eV (GW$_0$), respectively. Whereas it is larger at $-K$, which correspondingly is 0.816 eV, 1.141 eV, and 1.510 eV, leading to a gap difference of 0.080 eV, 0.258 eV and 0.192 eV, respectively. The mean value of the gaps at K and $-K$ with SOC is close to the gap without SOC. The gap difference is a combined effect of spin polarization and SOC. The conduction and valence edge states at the $\pm K$ valleys are found to be mainly contributed from the d_{z^2} and $d_{x^2-y^2} \pm i d_{xy}$ states of the V atom, respectively. Therefore, the z component of the orbital magnetic moment μ_L of the conduction and valence edge states at the $\pm K$ valleys is about 0 and $\pm 2\mu_B$, respectively. Here μ_B is the Bohr magneton. We have also calculated the mean value of spin of the valence band edge and found that $\langle \hat{\sigma}_x \rangle \approx \langle \hat{\sigma}_y \rangle \approx 0$ and $\langle \hat{\sigma}_z \rangle \approx 1$, where $\hat{\sigma}$ is the Pauli operator. The SOC in the V atom will induce an energy shift which is proportional to $\langle \hat{\sigma}_z \rangle \cdot \mu_L$. The conduction band edges in the valleys, in which $\mu_L \approx 0$, almost remain unshifted. Since μ_L is about $2\mu_B$ and $-2\mu_B$ at the valence band edge of the K and the $-K$ valleys, the SOC induces opposite energy shift in the valence band edges of the $\pm K$ valleys, giving rise to different energy gaps at the inequivalent valleys. The valley with a smaller gap is easier to be excited and the carrier occupancy is unequal at the two valleys, giving rise to valley polarization. The degree of valley polarization is also underestimated by PBE.

3.2. Berry curvature of Janus H-VSSe

In order to study the valleytronic properties of H-VSSe, on the basis of the energy band calculations, we calculate the Berry curvature and investigate the effect of SOC on it. It is found that when only the spin polarization is considered in the absence of SOC, the Berry curvatures at the K and $-K$ valleys are -11.28 Å^2 and 11.28 Å^2, respectively, which are of the same magnitude and opposite sign. Since the Berry curvature is an equivalent magnetic field in the momentum space, it can act on the moving carriers, and the opposite Berry curvature can lead to the valley Hall effect.[40] In the presence of SOC, as shown in Fig. 4(b), the Berry curvatures of H-VSSe at the two valleys K ($-K$) are -16.41 Å^2 and 9.09 Å^2, respectively. The signs are still opposite but the magnitudes are not equal, which can lead to anomalous valley Hall effect.[15] Therefore, H-VSSe is a potential magnetic valley material with intrinsic valley polarization.

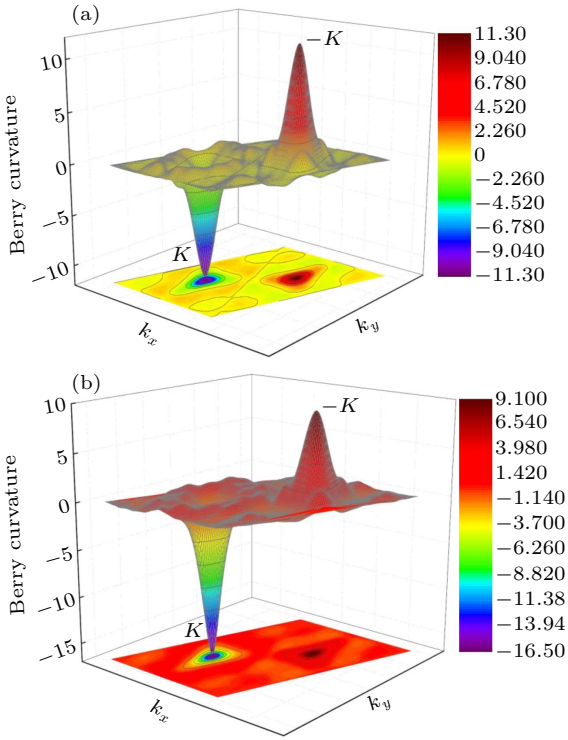


Fig. 4. The Berry curvature of Janus H-VSSe. Panel (a) with ferromagnetism and without SOC, panel (b) with ferromagnetism and SOC.

3.3. Excitonic effects of Janus H-VSSe

Optical excitation is an important means to excite the valley carriers. Usually, the 2D materials have relatively weak screening, and therefore the electron–hole interaction is strong, giving rise to large binding energy. In non-magnetic transition metal dichalcogenides such as MoS_2, it has been found both experimentally and theoretically that there are two exciton peaks in the photoluminescent spectrum. One corresponds to the A exciton formed by an electron in the bottom of the valley conduction band and a hole left in the top of the valley valence band. The other is B exciton formed by an electron in the bottom of the valley conduction band and a hole left in the second highest valence band in the valley.[41,42] The band structure of H-VSSe shown in Fig. 3 differs from that of MoS_2 significantly. It is interesting to know how the optical spectrum of H-VSSe would change due to its ferromagnetism.

To study the optical properties of H-VSSe, we calculate its dielectric function based on the GW_0 calculation. At first, only the spin polarization is considered without SOC. The optical transition will create an electron in the conduction band and leave a hole in the valence band. If the electrons and holes are free (no interaction), the excitation energy has to overcome the band gap (1.432 eV). As shown in Fig. 5, the first peak of the imaginary part of the GW-RPA dielectric function is located at 1.432 eV, which is the same as its corresponding quasiparticle bandgap. In reality, the electron–hole pair will be bound by Coulomb attraction to form a hydrogenic atom, i.e., exciton. In comparison with the free electron and hole state, the bounding electron–hole state has lower energy and therefore the excitation energy is lower than the band gap. The energy difference is the excitonic binding energy. In the GW-BSE spectrum, the first peak is red-shifted to 0.911 eV after the electron–hole attraction being taken into account, which corresponds to a binding energy of 0.521 eV. This first peak is split into two peaks around its old position (0.911 eV) after the inclusion of SOC. In contrast to MoS_2 and other similar materials, where the A and B excitonic peaks are due to the spin splitting in the same valley, the first two peaks of H-VSSe (red line in Fig. 5) are from the two inequivalent valleys with different gaps (Fig. 3). The splitting of the two peaks is different from the gap difference of the two inequivalent valleys.

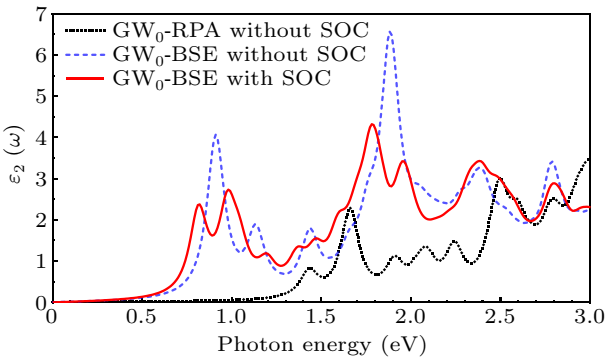


Fig. 5. The calculated imaginary parts of the complex dielectric function $\varepsilon_2(\omega)$ of H-VSSe on the k-grid of $15 \times 15 \times 1$. The black dotted, blue dashed and red solid lines are the spectra calculated by RPA without SOC, BSE without SOC and BSE with SOC on the top of the GW_0, respectively.

From Table 1, it can be seen that the valley with a larger band gap has larger excitonic binding energy. Based on the hydrogenic picture of excitons, the binding energy E_b of the electron–hole pair in the 2D systems is proportional to μ/ε^2, where μ and ε are the effective mass and dielectric constant.[43,44] The $k \cdot p$ theory points out that the effective masses of the electron and hole quasiparticles almost linearly depend on the energy gap.[43,45] Therefore, effective mass, energy gap and excitonic binding energy are proportional to each other. We calculate the electron and hole effective mass of the valleys using the k-grid of $15 \times 15 \times 1$. It is found that at the K valley, the calculated effective masses of the electron and hole are $3.80m_e$ and $4.09m_e$, respectively, where m_e is the rest mass of an electron. For the $-K$ valley with a larger band gap and larger excitonic binding energy (see Table 1), the corresponding calculated effective mass is larger, which are $5.09m_e$ and $5.05m_e$, respectively. Therefore, our calculations basically agree with the hydrogenic model and $k \cdot p$ theory.

Table 1. Quasiparticle bandgaps, band gap difference, BSE peaks, BSE peak splitting and exciton binding energies of the two inequivalent valleys for different k-grids.

H-VSSe	Valley	Band gap (eV)	Band gap difference (meV)	BSE peak (eV)	BSE peak splitting (meV)	Exciton binding energies (eV)
$6 \times 6 \times 1$	K	1.581	165	0.621	160	0.960
with SOC	$-K$	1.746		0.781		0.965
$9 \times 9 \times 1$	K	1.420	179	0.711	170	0.709
with SOC	$-K$	1.599		0.881		0.718
$12 \times 12 \times 1$	K	1.353	188	0.781	170	0.572
with SOC	$-K$	1.541		0.951		0.590
$15 \times 15 \times 1$	K	1.318	192	0.821	160	0.497
with SOC	$-K$	1.510		0.981		0.529
$15 \times 15 \times 1$	K	1.432	0	0.911	0	0.521
without SOC	$-K$	1.432		0.911		0.521
$15 \times 15 \times 1$	K	1.427	0	0.911	0	0.517
without SOC (400 eV)	$-K$	1.427		0.911		0.517

From a technical point of view, optical transition simulation needs to use a sufficiently dense k-point grid for integration over the irreducible Brillouin zone, therefore the convergence with respect to k-point sampling is very important. In order to reduce the calculation cost in GW-BSE calculations, we respectively use 400 eV and 300 eV as the plane wave cutoff energy. As shown in Table 1, it can be seen that for the non-SOC case with the k-grid of $15 \times 15 \times 1$, the 300 eV and 400 eV cutoffs yield basically the same results, with the band gaps of 1.432 eV and 1.427 eV and the exciton peak positions of 0.911 eV and 0.911 eV, respectively. Therefore, the cutoff is set to be 300 eV in our calculations. For H-VSSe, we have consider a series of k-grids of $6 \times 6 \times 1$, $9 \times 9 \times 1$, $12 \times 12 \times 1$ and $15 \times 15 \times 1$, and calculate the quasiparticle energy gaps and the positions of the excitonic peaks, as listed in Table 1. As the density of the k-grid increases, the band gap becomes smaller, the exciton peak gradually is blue-shifted. As a result, the calculated binding energy as the difference between the quasiparticle gap and the position of the first two excitonic peaks is also reduced simultaneously. The results in Table 1 show that good convergence has been achieved at the k-grid of $15 \times 15 \times 1$. It can also be observed in Table 1 and Fig. 6 that the difference of the gap at K and $-K$ is about 0.18 eV and the difference of the BSE peak positions is almost of the same value, both of which are almost invariant with respect to the k-grids. Table 1 also reveals that the $-K$ valley has a larger band gap and a larger excitonic binding energy, suggesting that a larger gap leads to weaker screening.

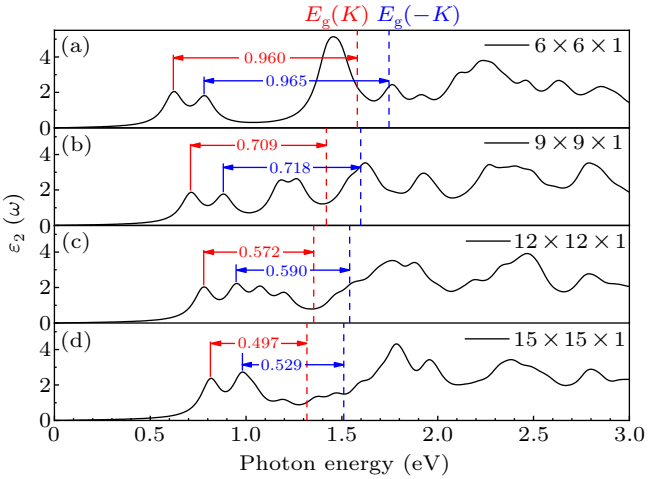


Fig. 6. The calculated imaginary parts of complex dielectric function $\varepsilon_2(\omega)$ of H-VSSe using different k-grids by BSE/GW method. The calculated spectra in panels (a)–(d) correspond to $6 \times 6 \times 1$, $9 \times 9 \times 1$, $12 \times 12 \times 1$ and $15 \times 15 \times 1$ k-grids, respectively. The red and blue dash lines denote the absorption peaks due to the optical transitions at valley K and $-K$ without considering the electron–hole interaction. The numbers give the exciton binding energy.

4. Conclusion

We have investigated the optical properties of a ferrovalley material, Janus H-VSSe, by first-principles calculations. To accurately calculate the band gap, the GW_0 method based on many body perturbation is used. Both PBE and GW calculations show that H-VSSe is ferromagnetic. The GW gaps are found to be about two times larger than the PBE gaps, suggesting strong many body effects. The band gaps at the two inequivalent valleys degenerate in the absence of the SOC, and they become different with one gap increasing and the other one decreasing after the SOC is turned on. On the top of the GW calculation, the BSE is solved to obtain the optical spectrum including the electron–hole interaction. The binding energy of the lowest BSE peak in the excitonic spectrum corresponding to the optical gap, is much lower than that of the quasiparticle GW gap, which proves that the exciton effect is strong in H-VSSe. This BSE peak is split into two peaks by SOC. The splitting is about the same as the difference of the GW band gaps at the two inequivalent valleys in the presence of SOC. Our results show that the band structure of ferrovalley Janus H-VSSe is very different from that of MoS_2. The two lowest BSE peaks in the optical spectrum of H-VSSe are from the two inequivalent valleys with different gaps, in contrast to the A and B exciton peaks of MoS_2 which are from the same valley.

Acknowledgments

Project supported by the National Natural Science Foundation of China (Grant No. 11874315) and the Postgraduate Scientific Research Innovation Project of Hunan Province of China (Grant No. CX20220663).

References

[1] Schaibley J R, Yu H, Clark G, *et al.* 2016 *Nat. Rev. Mater.* **1** 16055
[2] Choi W, Choudhary N, Han G H, *et al.* 2017 *Mater. Today* **20** 116
[3] Liu G B, Xiao D, Yao Y, *et al.* 2015 *Chem. Soc. Rev.* **44** 2643
[4] Qiu D Y, Da Jornada F H and Louie S G 2013 *Phys. Rev. Lett.* **111** 216805
[5] Ramasubramaniam A 2012 *Phys. Rev. B* **86** 115409
[6] Shi H, Pan H, Zhang Y W and Yakobson B I 2013 *Phys. Rev. B* **87** 155304
[7] Srivastava A, Sidler M, Allain A V, *et al.* 2015 *Nat. Phys.* **11** 141
[8] Liu W, Luo C, Tang X, *et al.* 2019 *AIP Adv.* **9** 045222
[9] Peng R, Ma Y, Zhang S, *et al.* 2018 *J. Phys. Chem. Lett.* **9** 3612
[10] Cheng Y C, Zhang Q Y and Schwingenschlögl U 2014 *Phys. Rev. B* **89** 155429
[11] Qi J, Li X, Niu Q and Feng J 2015 *Phys. Rev. B* **92** 121403
[12] Zhong D, Seyler K L, Linpeng X, *et al.* 2017 *Sci. Adv.* **3** e1603113
[13] Zhang A, Gong Z, Zhu Z, *et al.* 2020 *Phys. Rev. B* **102** 155413
[14] Zhang A, Yang K, Zhang Y, *et al.* 2021 *Phys. Rev. B* **104** L201403
[15] Tong W Y, Gong S J, Wan X and Duan C G 2016 *Nat. Commun.* **7** 13612
[16] Liu J, Hou W J, Cheng C, *et al.* 2017 *J. Phys. Condens. Matter* **29** 255501
[17] Zhao P, Ma Y, Lei C, *et al.* 2019 *Appl. Phys. Lett.* **115** 261605
[18] Cheng H, Zhou J, Ji W, *et al.* 2021 *Phys. Rev. B* **103** 125121
[19] Zhao P, Dai Y, Wang H, *et al.* 2022 *ChemPhysMater* **1** 56
[20] Hu H, Tong W Y, Shen Y H, *et al.* 2020 *NPJ Comput. Mater.* **6** 1
[21] Peng R, Ma Y, Xu X, *et al.* 2020 *Phys. Rev. B* **102** 035412
[22] Ding Y and Wang Y 2020 *Nanoscale* **12** 1002
[23] Liang L, Yang Y, Wang X and Li X 2023 *Nano Lett.* **23** 858
[24] Cui Q, Zhu Y, Liang J, *et al.* 2021 *Phys. Rev. B* **103** 085421
[25] Luo C, Peng X, Qu J and Zhong J 2020 *Phys. Rev. B* **101** 245416
[26] Li C and An Y 2022 *Phys. Rev. B* **106** 115417

[27] Wang L, Lin Z and An Y 2021 *J. Alloys Compd.* **854** 157141
[28] Zhang C, Nie Y, Sanvito S and Du A 2019 *Nano Lett.* **19** 1366
[29] Qi S, Jiang J and Mi W 2020 *Phys. Chem. Chem. Phys.* **22** 23597
[30] Zheng G, Zhang B, Duan H, *et al.* 2023 *Physica E* **148** 115616
[31] Zhao Y F, Shen Y H, Hu H, *et al.* 2021 *Phys. Rev. B* **103** 115124
[32] Yang J, Wang A, Zhang S, *et al.* 2018 *Phys. Chem. Chem. Phys.* **21** 132
[33] Mak K F, Lee C, Hone J, *et al.* 2010 *Phys. Rev. Lett.* **105** 136805
[34] Kresse G and Furthmüller J 1996 *Comput. Mater. Sci.* **6** 15
[35] Kresse G and Furthmüller J 1996 *Phys. Rev. B* **54** 11169
[36] Perdew J P, Burke K and Ernzerhof M 1996 *Phys. Rev. Lett.* **77** 3865
[37] Heyd J, Scuseria G E and Ernzerhof M 2003 *J. Chem. Phys.* **118** 8207
[38] Aryasetiawan F and Gunnarsson O 1998 *Rep. Prog. Phys.* **61** 237
[39] Pizzi G, Vitale V, Arita R, *et al.* 2019 *J. Phys. Condens. Matter* **32** 165902
[40] Olsen T and Souza I 2015 *Phys. Rev. B* **92** 125146
[41] Thomas A and Jinesh K B 2022 *ACS Omega* **7** 6531
[42] Lin Y, Ling X, Yu L, *et al.* 2014 *Nano Lett.* **14** 5569
[43] Choi J H, Cui P, Lan H and Zhang Z 2015 *Phys. Rev. Lett.* **115** 066403
[44] Harrison P and Valavanis A 2016 *Quantum wells, wires and dots: theoretical and computational physics of semiconductor nanostructures* 2nd edn. (Chichester: Wiley) p. 203
[45] Winkler R, Papadakis S, De Poortere E and Shayegan M 2003 *Spin-orbit coupling in two-dimensional electron and hole systems* (Berlin: Springer) p. 12